

## Localized corrosion mechanism associated with precipitates containing Mg in Al alloys

REN Wen-da(任文达)<sup>1,2</sup>, LI Jin-feng(李劲风)<sup>1,2</sup>, ZHENG Zi-qiao(郑子樵)<sup>1,2</sup>, CHEN Wen-jing(陈文敬)<sup>1,2</sup>

1. School of Materials Science and Engineering, Central South University, Changsha 410083, China

2. The Key Laboratory of Nonferrous Metal Materials Science and Engineering, Ministry of Education, Changsha 410083, China

Received 30 September 2006; accepted 8 December 2006

**Abstract:** To clarify the localized corrosion mechanism associated with precipitates containing Mg in Al alloys, the simulated bulk precipitates of  $S$  and  $\beta$  were synthesized through melting and casting. Their electrochemical behaviors and coupling behaviors with  $\alpha(\text{Al})$  in NaCl solution were measured. Meanwhile, simulated Al alloys containing  $S$  and  $\beta$  particles were prepared and their corrosion morphologies were observed. It's found that there exist two kinds of corrosion mechanisms associated with precipitates containing Mg. The precipitate of  $\beta$  is anodic to the alloy base, resulting in its anodic dissolution and corrosion during the whole corrosion process. While, there exists a corrosion conversion mechanism associated with the  $S$  precipitate, which contains active element Mg and noble element Cu simultaneously. At an initial stage,  $S$  is anodic to the alloy matrix at its periphery and the corrosion occurs on its surface. However, during its corrosion process, Mg is preferentially dissolved and noble Cu is enriched in the remnants. This makes  $S$  become cathodic to  $\alpha(\text{Al})$  and leads to anodic dissolution and corrosion on the alloy base at its periphery at a later stage.

**Key words:** localized corrosion mechanism; Mg-containing precipitate; Al alloy

### 1 Introduction

Magnesium is a widely used alloying element in commercial aluminum alloys. The electrochemical characteristics of second-phase particles containing Mg element often play an important role in understanding localized corrosion in aluminum alloys. The role of intermetallic compound(IMC) particles is often described in the context of their galvanic relationships with the surrounding matrix phase, solute-depleted zones or other IMC particles. Since 1940s, researchers have synthesized bulk analogs to facilitate measurement of corrosion potentials by conventional equipment. The galvanic relationships determined from measurement of analogs have formed an important part of microstructure-based models for localized corrosion, intergranular corrosion and stress corrosion cracking[1–2].

Due to their excellent combination of strength and corrosion resistance[3–4], wrought alloys of the 5XXX series Al alloys have been widely used in automobile body structures, shipbuilding and cryogenic vessels. The addition of Mg markedly increases the strength of these

alloys without a significant decrease of ductility. However, with Mg content increasing, Al-Mg alloys become susceptible to stress corrosion cracking due to super saturation of solid solution and increased tendency to precipitate  $\beta$  phases ( $\text{Al}_3\text{Mg}_2$ ) at grain boundaries[5–6].  $S(\text{Al}_2\text{CuMg})$  particles widely exist in Al-Cu-Mg-X alloys (Aluminum association 2XXX series) that are known for being prone to corrosion in common use. The inhomogeneous distribution of Cu in the alloy microstructure has been shown to be a major cause for low resistance to pitting and stress corrosion cracking. Specifically, the concentration of Cu in second-phase particles and the local depletion of Cu in certain microstructural regions establish local galvanic cells resulting in localized attack[7–8]. In this study, to compare the roles of these Mg-containing particles in corrosion process,  $S$  phase and  $\beta$  phase in bulk form were prepared for the measurement of corrosion potentials by conventional electrochemical equipment. Experiments were also conducted to understand the nature of the  $S$  phase- $\alpha(\text{Al})$  and  $\beta$  phase- $\alpha(\text{Al})$  matrix galvanic couples in NaCl solution and dissolution phenomena associated with Mg-containing phase particle during the corrosion

of Al alloys.

## 2 Experimental

### 2.1 Preparation analogs for bulk $S$ and $\beta$

The simulated bulk precipitates of  $S$  and  $\beta$  were manufactured by melting and casting according to their chemical proportion. The cast ingot for  $S$  was annealed at 420 °C for 24 h and that for  $\beta$  was annealed at 425 °C for 24 h. Portion of cast ingots were pulverized to generate powder suitable for X-ray powder diffraction(XRD). The alloy base is substituted by  $\alpha(\text{Al})$ , due to its little alloying element.

### 2.2 Potentiodynamic scanning curves of $S$ , $\beta$ and $\alpha(\text{Al})$

Specimens for electrochemical measurement were cut from  $\alpha(\text{Al})$  and the annealed simulation ingots, connected with a copper wire, and then mounted in epoxy resin with a surface exposed. The exposed surface was ground using abrasive papers, mechanical polished with  $\text{Cr}_2\text{O}_3$  powder, degreased with acetone, rinsed using distilled water and then dried in air. The corrosion medium was a neutral aerated 3.5% NaCl solution prepared using analytical NaCl and distilled water.

The potentiodynamic scanning curves of individual  $\alpha(\text{Al})$ ,  $\beta$  and  $S$  analogs were measured with a SI 1287 electrochemical interface in a three-compartment cell system. The working electrode was  $\alpha(\text{Al})$ ,  $\beta$  and  $S$  analog respectively. A thin sheet of platinum and saturated calomel electrode(SCE) with a Lugging capillary served as counter and reference electrodes respectively. During the potentiodynamic scanning curve measurement, cathodic polarization was carried out firstly, and then the anodic polarization. The scanning rate was 1 mV/s.

### 2.3 Coupling behavior and corrosion morphology of $S$ - $\alpha(\text{Al})$ and $\beta$ - $\alpha(\text{Al})$ coupled system

The  $S$  and  $\beta$  analogs were coupled with  $\alpha(\text{Al})$  in the NaCl solution respectively, as shown in Fig.1. In  $\beta$ - $\alpha(\text{Al})$  coupled system, the exposed area of  $\beta$  analog and  $\alpha(\text{Al})$  was 0.07 cm<sup>2</sup> and 0.15 cm<sup>2</sup> respectively. In  $S$ - $\alpha(\text{Al})$  coupled system, the exposed area of  $S$  phase and  $\alpha(\text{Al})$  was 0.07 cm<sup>2</sup> and 0.187 cm<sup>2</sup> respectively. During the coupled process, coupling current of  $S$ - $\alpha(\text{Al})$  and  $\beta$ - $\alpha(\text{Al})$  was measured. Ten days later, the coupling test was finished, the coupling was unraveled and the open circuit potential of corresponding electrode was measured with the SI 1287 Electrochemical interface. The corrosion products on the electrodes were removed by ultrasonic cleaning for 10 min and degreased in alcohol. The corrosion morphologies of the coupled specimen were observed with a KYKY2800 SEM.

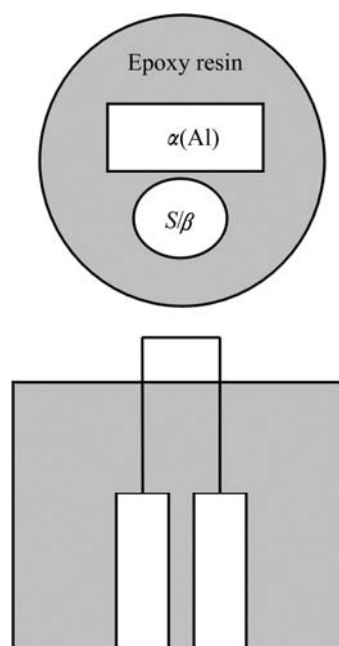


Fig.1 Schematic drawing of coupling system

### 2.4 Preparation of simulated Al alloys containing $S$ and $\beta$ phase particles and their corrosion morphology

Usually, the corrosion morphologies associated with aging precipitates could not be recognized by SEM due to their small size in Al alloys. In order to clearly observe the corrosion morphologies associated with them, LI et al[9] prepared simulated Al alloys from  $\alpha(\text{Al})$  and simulated aging precipitate particles through hot rolling. Here simulated alloys were made with  $\alpha(\text{Al})$  and the simulated precipitates of  $S$  and  $\beta$ . Two  $\alpha(\text{Al})$  plates with a thickness of 5 mm were polished and degreased in 50 g/L NaOH solution at 70 °C, then rinsed with water and dried in the air. The broken simulated precipitates of  $S$  and  $\beta$  were placed between them, and then they were rolled to 3 mm, as shown in Fig.2. The rolling temperature of  $S$ -containing alloy was 250 °C and  $\beta$ -containing alloy was 150 °C. The laminated plates were annealed at their rolling temperature respectively for 20 h. As a result, simulated Al alloys containing the  $S$  and  $\beta$  particles were formed respectively.

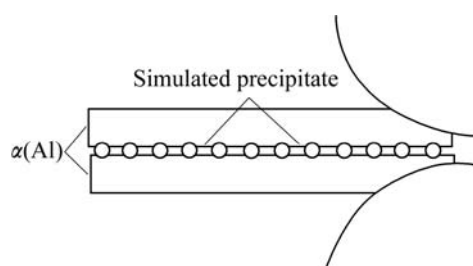
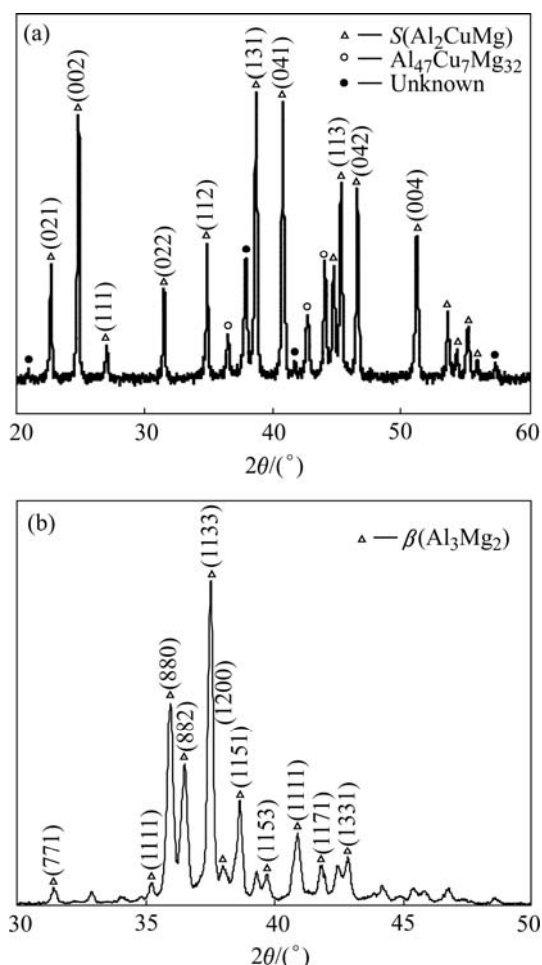


Fig.2 Simulated alloy process through rolling

The sectional surface of the simulated alloys was ground using abrasive papers until the tiny  $S$  and  $\beta$  phases embedded in the  $\alpha(\text{Al})$  can be observed, polished with  $\text{Cr}_2\text{O}_3$  powder, degreased with acetone, rinsed using distilled water. Then they were immersed in the 3.5% NaCl solution for 12 h. To clearly distinguish the corrosion morphology of the simulated alloys, the corrosion product covered on the surface was removed using a solution of 2% $\text{CrO}_3$ +5% $\text{H}_3\text{PO}_4$  at 80 °C, and the corresponding corrosion morphologies were observed with a KYKY2800 SEM.

### 3 Results and discussion

Fig.3 shows the XRD patterns of the annealed ingots corresponding to the chemical proportion of  $\beta$  and  $S$ . The observed main peak positions agree well with  $S$  phase reported in the reference. There only exist a small quantity of  $\text{Al}_{47}\text{Cu}_7\text{Mg}_{32}$  and other unknown phase in the  $S$  phase ingot, as seen in Fig.3(a). These discrepancies could be attributed to deviation in composition from the equilibrium composition.  $\beta$  phase is predominant phase in the corresponding ingot. So the simulated phases of  $S$



**Fig.3** XRD patterns of ingot corresponding to chemical proportion of  $S$ (a) and  $\beta$ (b)

and  $\beta$  can substitute for the real precipitates of  $S$  and  $\beta$  in Al alloys and undergo electrochemical measurements. Meanwhile, the alloy base around  $\beta$  and  $S$  can be substituted by  $\alpha(\text{Al})$ , due to its little alloying element.

The potentiodynamic scanning curves and corresponding corrosion parameters of the simulated bulk precipitates and  $\alpha(\text{Al})$  immersed in the 3.5% NaCl solution for 1 h are presented in Fig.4 and Table 1 respectively. It is clearly seen that the corrosion potential ( $\varphi_{\text{corr}}$ ) of both  $S$  and  $\beta$  is negative with respect to that of  $\alpha(\text{Al})$ . The polarization of resistance ( $R_p$ ) of individual  $S$  and  $\beta$  is much less than that of  $\alpha(\text{Al})$ . Meanwhile, the corrosion current density ( $J_0$ ) of  $S$  and  $\beta$  is greater than that of  $\alpha(\text{Al})$ , indicating that  $S$  and  $\beta$  are more susceptible to corrosion at the beginning stage of immersion.

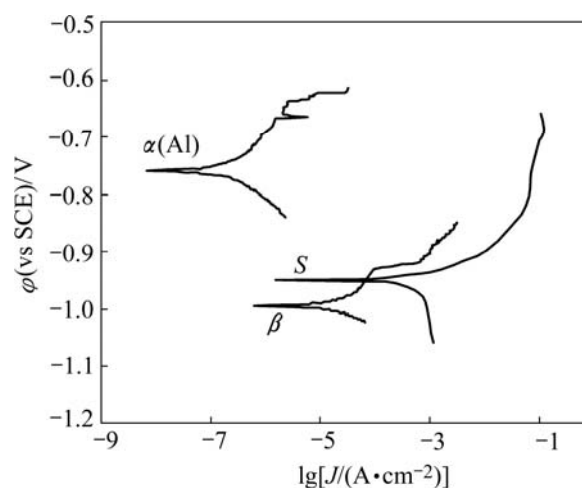


**Fig.4** Potentiodynamic scanning curves of individual  $S$ ,  $\beta$  and  $\alpha(\text{Al})$  in 3.5%NaCl solution

**Table 1** Corrosion parameters of simulated  $S$ ,  $\beta$  and  $\alpha(\text{Al})$  in 3.5%NaCl solution

Phase	$\varphi_{\text{corr}}(\text{vs SCE})/\text{V}$	$J_0/(\text{A}\cdot\text{cm}^{-2})$	$R_p/(\Omega\cdot\text{cm}^2)$
$\alpha(\text{Al})$	-0.759 1	$4.015 \times 10^{-7}$	$6.498 \times 10^5$
$\beta$	-0.993 7	$2.2768 \times 10^{-6}$	11457.6
$S$	-0.948 6	$1.43 \times 10^{-3}$	18.324

After coupling for 10 d, the order of the open circuit potential (OCP) of the simulated  $S$  and  $\alpha(\text{Al})$  changes. Compared with that at the beginning, the potential of  $S$  moves to a positive direction, resulting in the phenomenon that the potential of the simulated  $S$  is positive with respect to that of  $\alpha(\text{Al})$ , as seen in Fig.5(a). While, it is found that the open circuit potential of  $\beta$  is still negative with respect to that of  $\alpha(\text{Al})$  in the  $\beta$ - $\alpha(\text{Al})$  coupled system, as shown in Fig.5(b).

The potential of  $S$  moving towards the positive direction can be explained by the preferential dissolution of Mg from  $S$  and the enrichment of Cu on  $S$  surface. Compared with that at beginning, the content of Mg and

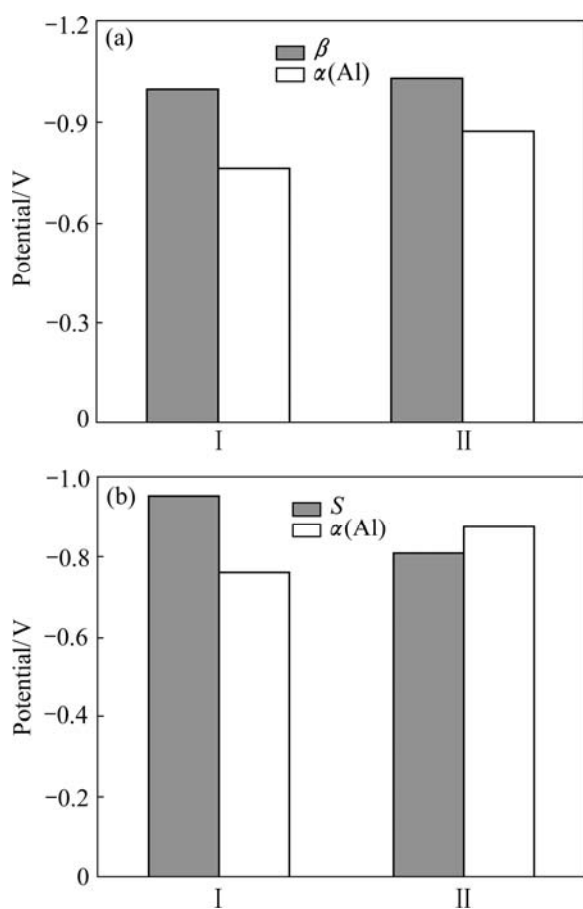


**Fig.5** Open circuit potential variation of corresponding electrode in  $\beta$ - $\alpha(\text{Al})$  (a) and  $S$ - $\alpha(\text{Al})$  (b) coupled system ( I At beginning; II 10 d later)

Al, especially Mg is greatly decreased, while the relative content of Cu is greatly increased, as shown in Fig.6.

The preferential dissolution phenomenon was found by BUCHHEIT et al[10] and SHAO et al[11] in  $S$  particles. When 2XXX series Al alloy containing  $S(\text{Al}_2\text{CuMg})$  particle is immersed in NaCl solution, active Mg is dissolved vigorously, resulting in porous Cu-rich remnants[12–14]. It is also found that when 6XXX series Al alloy is exposed to 0.1 mol/L phosphoric acid (pH=1.6), Mg is preferentially dissolved, resulting in Si-rich remnants in the  $\text{Mg}_2\text{Si}$  particles[15]. In this case, during the corrosion of  $S$ , active Mg is preferentially dissolved and the noble Cu is enriched on the electrode surface. It's reasonable to deduce that the potential of  $S$  will move to a positive direction. As a result, the corroded  $S$  will become cathodic to  $\alpha(\text{Al})$ . This phenomenon of electrode conversion from anode to cathode is also found in  $T_1(\text{Al}_2\text{CuLi})$  precipitate in Al-Li alloy[9], which contains active element Li and noble element Cu simultaneously.

The potential change in  $S$ - $\alpha(\text{Al})$  coupled system will cause the coupling current variation. At the initial stage of

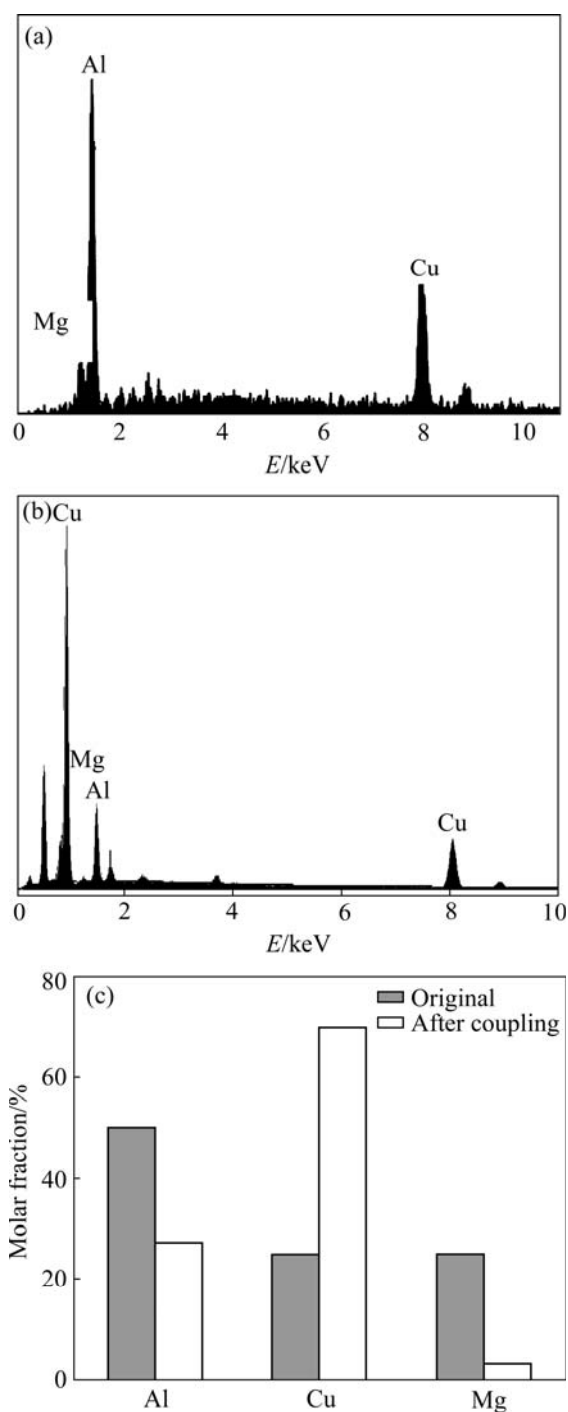


**Fig.6** Energy spectrum of simulated bulk  $S$  phase: (a) Original; (b) After coupling for 10 d; (c) Relative element content comparison of simulated bulk  $S$  phase before and after coupling

60 h,  $S$  endures anodic current in the coupled system. With immersion process going on, as the potential of  $S$  becomes positive with respect to that of  $\alpha(\text{Al})$ , the anodic current of  $S$  changes to cathodic current and increases, as seen in Fig.7. While in the  $\beta$ - $\alpha(\text{Al})$  coupled system, the potential of  $\beta$  is always negative with respect to that of  $\alpha(\text{Al})$ , and it endures anodic current in the whole process, as seen in Fig.7.

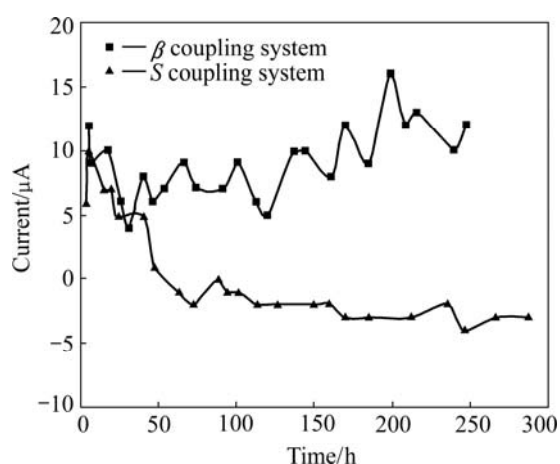


**Fig.7** Coupling current vs time for  $S$ - $\alpha$ (Al) system and  $\beta$ - $\alpha$ (Al) system

The attacked electrode surface morphologies of  $S$  and  $\beta$  after coupling for 10 d are presented in Fig.8. It is clearly seen that the smooth surface of  $S$  and  $\beta$  becomes very rough, indicating that severe corrosion occurs on  $S$  and  $\beta$  phases. Although corrosion also occurs on  $\alpha$ (Al) coupled with them, the corrosion degree is superficial, of which the corrosion morphologies are omitted.

Fig.9 shows the original optical morphologies of the simulated alloys. The simulated  $S$  and  $\beta$  are surrounded by  $\alpha$ (Al) and no obvious crevices are found between  $\alpha$ (Al) and the simulated phases. The corrosion morpho-

logies of the simulated alloys immersed in the NaCl solution for 12 h are presented in Fig.10. It is clearly seen that corrosion occurs on  $S$  and  $\beta$ . Fig.10(a) shows that  $\beta$  phases have been dissolved completely, only leaving corrosion pores in the Al base. The  $\alpha$ (Al) on the edge of  $\beta$  phases presents sharp outlines of corroded  $\beta$  phases, which means that no corrosion occurs on it. The potentiodynamic scanning curves show that  $\beta$  phase is more susceptible to corrosion (Fig.4), and the coupling behavior of  $\beta$ - $\alpha$ (Al) system demonstrates that  $\beta$  is always anodic to  $\alpha$ (Al) (Fig.5 and Fig.7). So it can be concluded that in the corrosion process, the tinny simulated  $\beta$  phases act as anodic phase and finally dissolve completely.

Fig.10(b) shows a backscatter electron image(BEI) of the corrosion surface of the simulated alloy containing  $S$  particle. The BEI shows a cloven structure in the corroded  $S$  particle, indicating that the severe corrosion occurs on the surface of  $S$  phase. Moreover, corrosion also occurs on the alloy matrix at its adjacent periphery. This phenomenon is consistent with the above potentiodynamic scanning curves and coupling behavior in  $S$ - $\alpha$ (Al) system. At an initial stage,  $S$  is anodic to the alloy matrix at its periphery (seen in Fig.4). This means that corrosion occurs on the surface of  $S$  firstly. However, with the corrosion going on, Mg element in  $S$  is preferentially dissolved and noble Cu is enriched in the remnants. This dealloying phenomenon is confirmed by

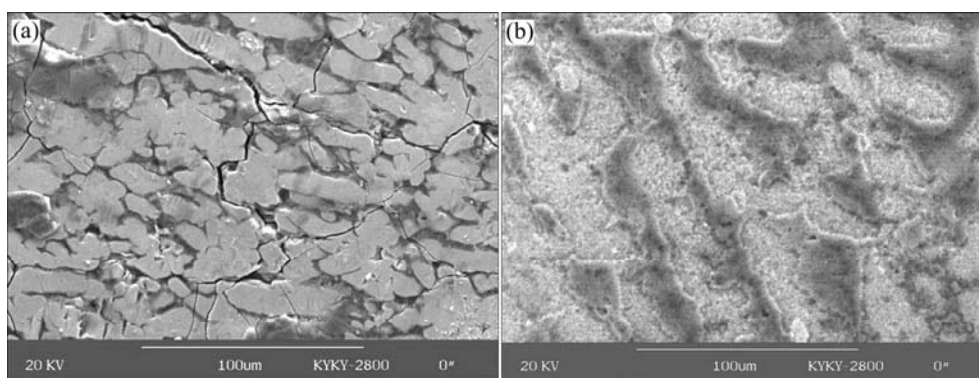


**Fig.8** Representative corrosion morphologies of  $S$  in  $S$ - $\alpha$ (Al) system (a) and  $\beta$  in  $\beta$ - $\alpha$ (Al) system (b) coupled in 3.5% NaCl solution for 10 d

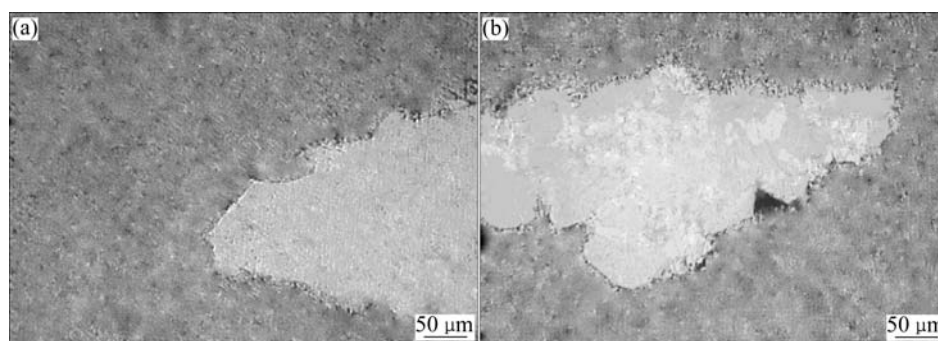


**Fig.9** Optical photographs of  $\beta$ -containing simulated alloy (a) and  $S$ -containing simulated alloy (b)

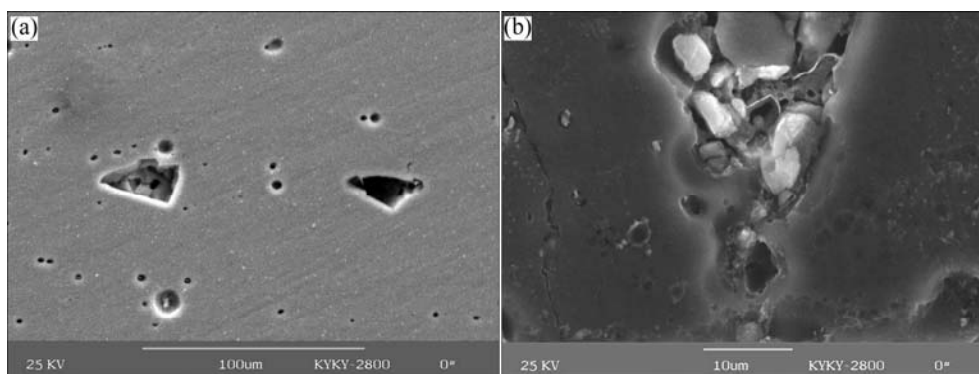


**Fig.10** Corrosion morphologies of  $\beta$ -containing simulated alloy (a) and  $S$ -containing simulated alloy (b) immersed in NaCl solution for 12 h

the energy spectrum of the coupled  $S$  (seen in Fig.6). Additionally, BEI also shows this phenomenon. Because backscattering efficiency scales with the atomic number of the scattering atom, which means that regions containing heavy elements will appear brighter than regions of lower average atomic number. In this case, the BEI in Fig.10(b) shows that some parts of  $S$  phase remnant are obviously brighter than the base, implicating Cu-rich remnant left. At this stage, the potential of  $S$  moves to the positive direction gradually and finally becomes cathodic to  $\alpha(\text{Al})$ . The variation of coupling current of the  $S$ - $\alpha(\text{Al})$  system in Fig.7 shows this process. As a result, the anodic dissolution and corrosion occur on the alloy matrix at its adjacent periphery.

## 4 Conclusions

1) There are two corrosion mechanisms associated with precipitates containing Mg in Al alloy. The  $\beta$  precipitate is anodic to the alloy base at its adjacent throughout the whole corrosion process. So the anodic dissolution and corrosion only occur on its surface.

2) There exists corrosion conversion mechanism associated with  $S$  precipitate, which contains active element Mg and noble element Cu synchronously. At an initial stage,  $S$  is anodic to the alloy matrix at its periphery and the corrosion occurs on its surface. However, with corrosion going on, Mg element in  $S$  is preferentially dissolved and noble Cu is enriched in the remnants. This process drives the potential of  $S$  moving to a positive direction and finally  $S$  phase becomes cathodic to  $\alpha(\text{Al})$ , which results in the anodic dissolution and corrosion of Al base at its periphery at later stage.

## References

[1] GAVALÉ J R, DEMICHELI S M. Mechanism of intergranular corrosion of Al-Cu alloys [J]. Corrosion Science, 1970, 10(11):

795–807.  
 [2] MULLER I L, GALVELE J R. Pitting potential of high purity binary aluminum alloys—I. Al-Cu alloys. Pitting and intergranular corrosion [J]. Corrosion Science, 1977, 17(3): 179–193.  
 [3] WANG Zhu-tang, TIAN Rong-zhang. Aluminum Alloys and Process Handbook [M]. Changsha: Central South University Press, 2001, (in Chinese).  
 [4] DAVIS J R. Corrosion of aluminum and aluminum alloys [M]. OH, USA: ASM International, Materials Park, 1999.  
 [5] SUMMERSON T J, SPROWLS D O. Corrosion behavior of aluminium alloys [C]// STARKE E A Jr, SANDERS T H Jr. Proceedings of Aluminium alloys—Their Physical and Mechanical Properties, Vol III. Warley, UK: EMAS Ltd, 1986: 1175–1162.  
 [6] SAMPATH D, MOLDENHAUER S, SCHIPPER H R, MECHSNER K HASZLER A. decomposition of solid solution of the AA5083 alloy upon exposure to elevated temperatures [J]. Materials Science Forum, 2000, 331/337: 1089–1094.  
 [7] GARNER A, TROMANS D. Direct observation of intergranular corrosion in Al-4wt%Cu alloy [J]. Corrosion, 1979, 35(2): 55–60.  
 [8] URISHINO K, SUGIMOTO K. Stress-corrosion cracking of aged Al-Cu-Mg alloys in NaCl solution [J]. Corrosion Science, 1979, 19(4): 225–229.  
 [9] LI Jin-feng, LI Shi-chen, ZHENG Zi-qiao, CHEN Wen-jing, ZHAO Xu-shan. Simulation on function mechanism of  $T_1(\text{Al}_2\text{CuLi})$  precipitate in localized corrosion of Al-Cu-Li alloy [J]. Trans Nonferrous Met Soc China, 2006, 16(6): 1268–1273.  
 [10] BUCHHEIT R G, BOGER R K, CORROLL M C, LEARD R M, PAGLIA C, SEARLES J L. The electrochemistry of intermetallic particles and localized corrosion in Al alloys [J]. JOM, 2001, 53(7): 29–33.  
 [11] SHAO M H, FU Y, HU R G, LIN C J. A study on pitting corrosion of aluminum alloy 2024-T3 by scanning microreference electrode technique [J]. Materials Science and Engineering A, 2003, 344(1/2): 323–327.  
 [12] BUCHHEIT R G, GRANT R P, HLAVA P F, MCKENZIE B, ZENDER G L. Local dissolution phenomena associated with  $S$  phase ( $\text{Al}_2\text{CuMg}$ ) particles in aluminum alloy 2024-T3 [J]. Journal of the Electrochemical Society, 1997, 144(8): 2621–2627.  
 [13] BIRBILIS N, BUCHHEIT R G. Electrochemical characteristic of intermetallic phases in aluminum alloys [J]. Journal of the Electrochemical Society, 2005, 152(4): B140–B151.  
 [14] ZHU D O, VAN OOIJ W J. Corrosion protection of AA2024-T3 by bis-[3-(triethoxysilyl) propyl] tetra sulfide in neutral sodium chloride solution [J]. Corrosion Science, 2003, 45(10): 2163–2175.  
 [15] MIZUUNNO K, NYLUND A, OLEFJORD I. Surface reactions during pickling of aluminum-magnesium-silicon alloy in phosphoric acid [J]. Corrosion Science, 2001, 43(2): 381–396.

(Edited by YANG Bing)